ORGANOMETALLICS

pubs.acs.org/Organometallics Article

# Synthesis and Characterization of 2,2-Dimethylpent-4-en-1-yl Complexes of Rhodium and Iridium: Reversible Olefin Decomplexation and C−H Bond Activation

Sumeng Liu and Gregory S. Girolami*

Cite This: *Organometallics* 2021, 40, 714−724 Read Online

ACCESS | Metrics & More | Article Recommendations | Supporting Information

**ABSTRACT:** We describe the synthesis and characterization of four $\eta^1,\eta^2$-2,2-dimethylpent-4-en-1-yl complexes of stoichiometry $M(CH_2CMe_2CH_2CH{=}CH_2)$(diene), where M is Rh or Ir, and the diene is dibenzo[a,e]cyclooctatetraene (DBCOT), 1,5-cyclooctadiene (COD), or norbornadiene (NBD). All these compounds have four-coordinate square-planar structures. We also prepared a binuclear complex $[Ir(CH_2CMe_2CH_2CH{=}CH_2)(DBCOT)]_2(C_{14}H_{26})$, in which the iridium centers are five-coordinate owing to the presence of a bridging diolefin ligand. In all five complexes, the C=C bond of the pentenyl ligand reversibly decomplexes in solution so that the two faces of the olefin are exchanged; for $Rh(CH_2CMe_2CH_2CH{=}CH_2)$(DBCOT) (**2**), the activation parameters for olefin decomplexation are $\Delta H^{\ddagger}$ = 19 ± 1 kcal·mol$^{-1}$ and $\Delta S^{\ddagger}$ = 8 ± 4 cal·mol$^{-1}$ K$^{-1}$. Spin saturation transfer studies show that the decomplexation preserves the broken symmetry of the DBCOT ligand, which suggests that the olefin decomplexation in **2** most likely occurs by means of a C−H $\sigma$-complex, or, less likely, a T-shaped intermediate which is too short-lived for the alkyl group to migrate to the vacant coordination site. When this Rh compound is heated in solution, a C−H bond on the $\gamma$-carbon of the pentenyl ligand is activated to form a substituted $\eta^3$-allyl complex $Rh(\eta^3$-*anti*-$CH_2{=}CHCHCMe_3)$(DBCOT), which subsequently isomerizes in solution to form the more stable $Rh(\eta^3$-*syn*-$CH_2{=}CHCHCMe_3)$(DBCOT).

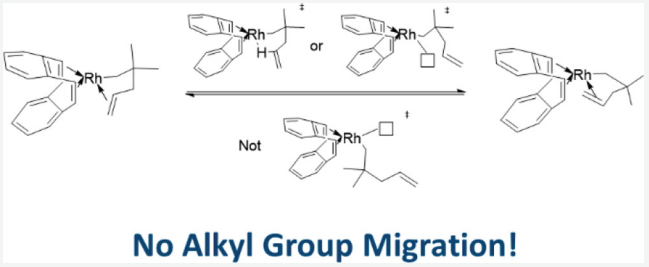


## INTRODUCTION

Films of noble metals grown by chemical vapor deposition (CVD)[1,2] often suffer from high surface roughness,[1] which is the result of poor nucleation (due to low surface reactivity) combined with autocatalytic growth on the nuclei that do form (owing to the highly catalytic nature of noble metals)[3,4] High surface roughness can potentially be avoided by employing a precursor whose ligands can more easily eliminate on the bare substrate,[5,6] and that also can temporarily poison the noble metal surface and reduce its reactivity.

We recently synthesized a platinum(II) pentenyl complex, *cis*-bis($\eta^1,\eta^2$-2,2-dimethylpent-4-en-1-yl)platinum, $Pt(CH_2CMe_2CH_2CH{=}CH_2)_2$, which exhibits this behavior: when this compound is used as CVD precursor, nucleation occurs readily and the resulting Pt films are highly smooth.[3,4] In solution, this compound readily undergoes decomplexation of a C=C bond from the metal center to form a highly reactive pseudo-three-coordinate platinum intermediate,[7,8] and it is likely that this olefin decomplexation process is responsible for the low barrier of nucleation seen for $Pt(CH_2CMe_2CH_2CH{=}CH_2)_2$ under CVD conditions.

In an effort to extend these findings, we became interested in preparing pentenyl complexes of other noble metals. Here we report the synthesis and characterization of rhodium(I) and iridium(I) complexes of stoichiometry $M(\eta^1,\eta^2$-2,2-dimethylpent-4-en-1-yl)(diene), studies of their dynamic processes in solution, and their transformations on being heated. Although these compounds are not sufficiently thermally stable to be useful as CVD precursors, the results provide deeper understanding of the nature of metal complexes of a relatively little-studied ligand class: chelating pentenyl groups.

## RESULTS

**Synthesis of $M(CH_2CMe_2CH_2CH{=}CH_2)$(diene) Complexes.** Treatment of the rhodium(I) starting material $[RhCl(diene)]_2$ with 1 equiv of (2,2-dimethylpent-4-en-1-yl)lithium[9] or the corresponding Grignard reagent[3] in THF affords a series of monomeric complexes of stoichiometry $Rh(CH_2CMe_2CH_2CH{=}CH_2)$(diene), compounds **1**-**3**, in which the diene is 1,5-cyclooctadiene (COD), dibenzo[a,e]-cyclooctatetraene (DBCOT), or norbornadiene (NBD), respectively (Scheme 1). The lithium reagent is preferred

Received: December 22, 2020
Published: March 8, 2021

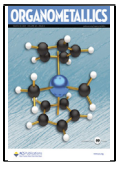






https://dx.doi.org/10.1021/acs.organomet.0c00798
*Organometallics* 2021, 40, 714−724

**Scheme 1. Synthesis of $M(CH_2CMe_2CH_2CH{=}CH_2)$(diene) Complexes**

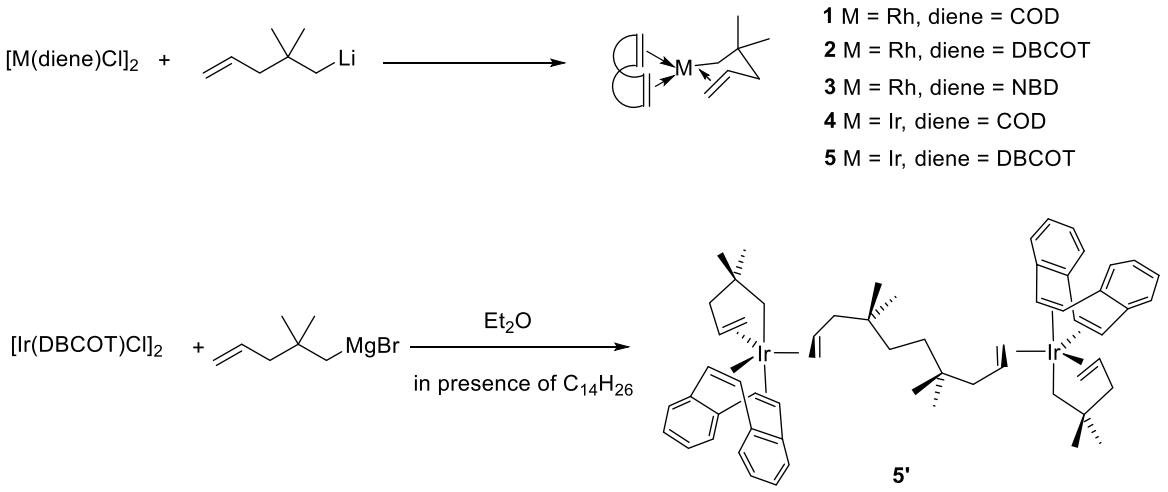


over the Grignard reagent because its synthesis from the corresponding pentenyl bromide is accompanied by the formation of smaller amounts of the pentenyl homocoupling product 4,4,7,7-tetramethyldeca-1,5-diene.

The reaction of the iridium(I) reagent $[IrCl(COD)]_2$ with (2,2-dimethylpent-4-en-1-yl)lithium gives the analogous complex $Ir(CH_2CMe_2CH_2CH{=}CH_2)(COD)$ (**4**). In contrast, $Ir(CH_2CMe_2CH_2CH{=}CH_2)(DBCOT)$ cannot be synthesized by treating $[IrCl(DBCOT)]_2$ with the lithium reagent in THF; because of the low solubility[10] of $[IrCl(DBCOT)]_2$, the lithium reagent reacts with THF instead. Treatment of $[IrCl(DBCOT)]_2$ with the lithium reagent in pentane, a solvent with which the lithium reagent does not react, gives a mixture of brown and white solids, with an overall formula of $Ir(CH_2CMe_2CH_2CH{=}CH_2)(DBCOT)\cdot 0.57C_7H_{14}$ (**5**). We suggest that the brown solid is the 4-coordinate $Ir(CH_2CMe_2CH_2CH{=}CH_2)(DBCOT)$, whereas the white solid is the 5-coordinate olefin adduct $Ir(CH_2CMe_2CH_2CH{=}CH_2)(DBCOT)(CH_2{=}CHCH_2CMe_3)$, in which the bound 4,4-dimethylpent-1-ene ligand is generated during the synthesis by reaction of some of the pentenyl groups with adventitious water. The suggested identifications of these compounds are supported by the $^1H$ NMR and mass spectra of **5** (Supporting Information (SI) Figures S3.20 and S3.25), and the isolation of a related 5-coordinate olefin adduct that is also colorless (see below).

Efforts to synthesize $Ir(CH_2CMe_2CH_2CH{=}CH_2)(DBCOT)$ from the 2,2-dimethylpent-4-en-1-yl Grignard reagent resulted in the isolation of colorless crystals of the five-coordinate iridium species $[Ir(CH_2CMe_2CH_2CH{=}CH_2)(DBCOT)]_2(C_{14}H_{26})$ (**5′**). This compound is the 2:1 adduct of $Ir(CH_2CMe_2CH_2CH{=}CH_2)(DBCOT)$ with 4,4,7,7-tetramethyldeca-1,9-diene, in which $C_{14}H_{26}$ is the homo coupling product of the pentenyl group; as mentioned above, this diene is generated during the synthesis of the Grignard reagent from the pentenyl bromide. As will be seen from the crystal structure below, each of the C=C bonds in 4,4,7,7-tetramethyldeca-1,9-diene coordinates to a different iridium center. Our observations are consistent with the behavior of other iridium DBCOT complexes, which tend to bind olefins to form five-coordinate species.[10]

The DBCOT compounds **2** and **5** are nonvolatile solids, whereas the COD and NBD compounds **1**, **3**, and **4** are thermally sensitive low melting oils. The latter are volatile and distill under vacuum (10 mTorr) with gentle heating (35 °C), but the distillation yields are poor because some decomposition occurs. Compound **5′** is unstable at room temperature: it dissociates to **5** and free 4,4,7,7-tetramethyldeca-1,9-diene.

**Crystal Structure of the $M(CH_2CMe_2CH_2CH{=}CH_2)$(diene) Complexes.** Crystal data for the rhodium DBCOT complex **2**, the iridium COD complex **4**, and the binuclear iridium DBCOT compound **5′** are given in SI Table S2.1, and bond distances and angles are summarized in Table 1. All

**Table 1. Selected Bond Distances for the $\eta^1,\eta^2$-2,2-Dimethylpent-4-en-1-yl Complexes of Rhodium and Iridium**

| | **2** | **4** | **5′** | $C_{14}H_{26}$ in **5′** |
|---|---|---|---|---|
| C=C /Å | 1.368(2) | 1.382(6) | 1.403(4) | 1.384(4) |
| M–$C_\alpha$ /Å | 2.0767(15) | 2.089(4) | 2.119(3) | |
| M–$C_{olefin}$[a] /Å | 2.3312(14) | 2.229(4) | 2.207(3) | 2.347(3) |
| M–$C_{olefin}$[b] /Å | 2.2592(15) | 2.197(4) | 2.220(3) | 2.263(3) |
| C=$C_{diene}$[c] /Å | 1.415(2) | 1.399(5) | 1.444(4)[e] | |
| C=$C_{diene}$[d] /Å | 1.387(2) | 1.398(5) | 1.399(4) | |
| M–$C_{diene}$[c] /Å | 2.1220(14) | 2.142(3) | 2.147(3)[e] | |
| | 2.1416(14) | 2.159(3) | 2.154(3)[e] | |
| M–$C_{diene}$[d] /Å | 2.2561(14) | 2.200(4) | 2.258(3) | |
| | 2.2468(15) | 2.183(4) | 2.299(3) | |

[a]Methine carbon. [b]Methylene carbon. [c]cis to alkyl. [d]trans to alkyl. [e]Equatorial C=C bond.

C=C bond distances are similar to or longer than the 1.366(3) Å distance seen for $Pt(CH_2CMe_2CH_2CH{=}CH_2)_2$,[3] suggesting that the C=C bonds are relatively weakly coordinated to their respective metal centers.

Compounds **2** and **4** are monomeric square-planar four-coordinate complexes (Figures 1 and 2). Consistent with the strong trans influence of alkyl groups,[11] for the diene ligand the M–C distances trans to the alkyl group are longer than those trans to the pentenyl C=C bond. For the same reason, in the diene ligand the C=C bond distances trans to the alkyl group are shorter than those trans to the pentenyl C=C bond (Table 1).

As seen in the platinum analog $Pt(CH_2CMe_2CH_2CH{=}CH_2)_2$, the rings formed by the pentenyl groups in **2** and **4** adopt chair conformations, in which the C=C bond vector of the pentenyl ligand is significantly tilted away from being


https://dx.doi.org/10.1021/acs.organomet.0c00798
Organometallics 2021, 40, 714−724

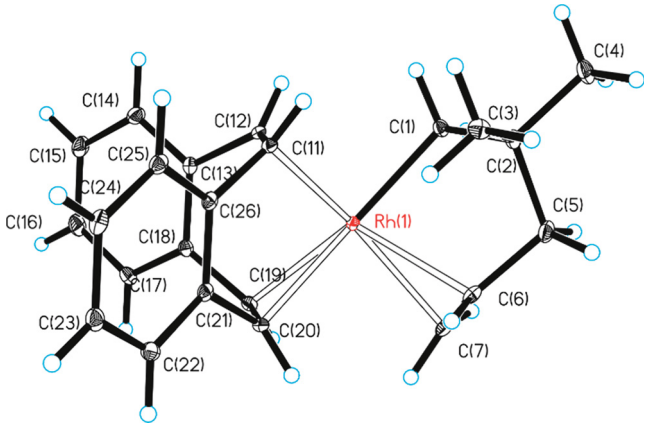


**Figure 1.** Molecular structure of (dibenzo[*a*,*e*]cyclooctatetraene)-($\eta^1$,$\eta^2$-2,2-dimethylpent-4-en-1-yl)rhodium(I) (**2**). Ellipsoids are drawn at the 35% probability level, except for hydrogen atoms, which are represented by arbitrarily sized spheres.

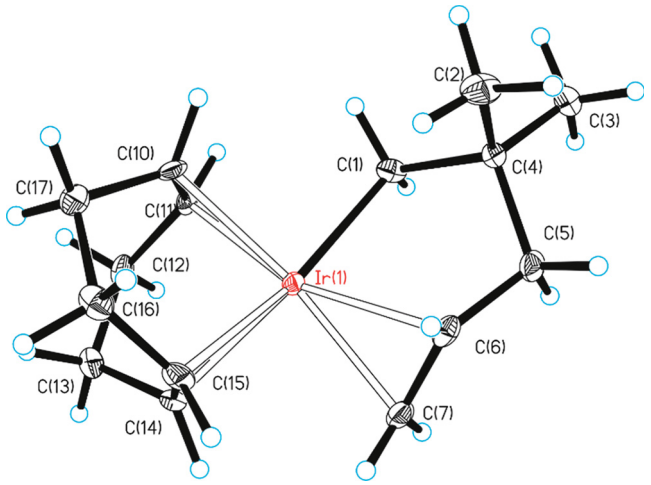


**Figure 2.** Molecular structure of (1,5-cyclooctadiene)($\eta^1$,$\eta^2$-2,2-dimethylpent-4-en-1-yl)iridium(I) (**4**). Ellipsoids are drawn at the 35% probability level, except for hydrogen atoms, which are represented by arbitrarily sized spheres.

perpendicular to the square plane. Notably, the DBCOT C═C bonds in **2** are parallel to one another due to its steric rigidity, whereas the COD C═C bonds in **4** are slightly tilted: the COD C═C bond trans to the alkyl group is twisted slightly toward being parallel to the pentenyl C═C bond, presumably to reduce steric clashing, as seen for the cis C═C bonds in $Pt(CH_2CMe_2CH_2CH{=}CH_2)_2$.[3]

Unlike **2** and **4**, compound **5′** is a dimer bridged by 4,4,7,7-tetramethyldeca-1,9-diene, the pentenyl bromide homocoupling product that is generated during the synthesis of the Grignard reagent used to make **5′**. The ligands around the iridium center are best viewed in terms of a trigonal bipyramidal coordination geometry, in which the pentenyl and DBCOT groups bridge between axial and equatorial sites (the alkyl end of the pentenyl group being axial), and one end of the 4,4,7,7-tetramethyldeca-1,9-diene occupies an equatorial site (Figure 3).

The six olefinic carbon atoms in the three equatorial sites are essentially coplanar with one another, whereas the axial C═C bond vector is parallel to this plane. To achieve this geometry, the ring formed by the pentenyl group adopts a boat conformation, instead of the chair conformation seen for the compounds above and for some related four-coordinate compounds.[3,12] A trigonal bipyramidal geometry with similar orientations of the C═C bonds has also been seen in one other five-coordinate complex in which four olefins coordinate to the iridium center;[13] in contrast, $IrCl(COD)_2$ adopts a square pyramidal geometry.[14]

**Structure and Bonding of the M($CH_2CMe_2CH_2CH{=}CH_2$)(diene) Complexes in Solution.** Overall, the NMR data suggest that **1**−**5** are unimolecular in solution, and adopt square planar structures like those seen in the solid state for **2** and **4**. The $^1$H and $^{13}$C NMR resonances in **1**−**5** have been assigned based on the peak patterns and coupling constants, NOESY NMR data, and comparisons with the $^1$H and $^{13}$C NMR spectra of the related platinum compound Pt-$(CH_2CMe_2CH_2CH{=}CH_2)_2$.[3] For all five compounds, there are four different olefinic CH resonances due to the coordinated diene (Figure 4); the fact that these groups are all chemically inequivalent clearly shows that in solution the pentenyl groups are coordinated to the metal center in an $\eta^1$,$\eta^2$ fashion (Table 2).[3] This conclusion is also supported by the

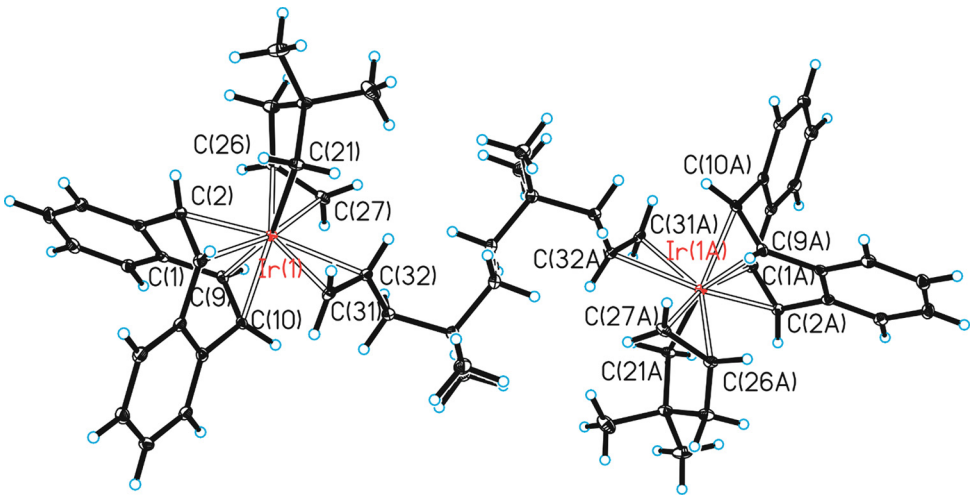


**Figure 3.** Molecular structure of bis{(dibenzo[*a*,*e*]cyclooctatetraene)($\eta^1$,$\eta^2$-2,2-dimethylpent-4-en-1-yl)iridium(I)}($\mu$-4,4,7,7-tetramethyldeca-1,9-diene) (**5′**). Ellipsoids are drawn at the 35% probability level, except for hydrogen atoms, which are represented by arbitrarily sized spheres.


https://dx.doi.org/10.1021/acs.organomet.0c00798
*Organometallics* 2021, 40, 714−724

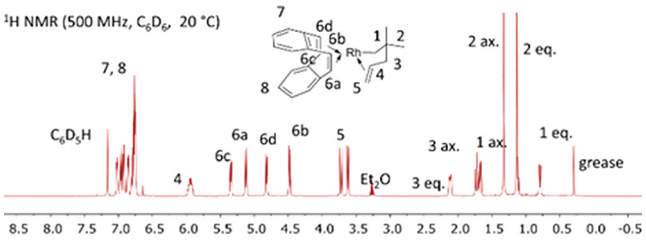


**Figure 4.** $^1$H NMR spectrum of (dibenzo[*a*,*e*]cyclooctatetraene)-($\eta^1$,$\eta^2$-2,2-dimethylpent-4-en-1-yl)rhodium(I) (**2**). Four different olefinic DBCOT resonances are observed due to the symmetry-breaking caused by chelation of the pentenyl ligand. The chemical shifts and coupling patterns of the protons on the pentenyl group are consistent with the structure in the solid state.

diminished $^3J_{HH}$ coupling constants seen for the −CH=CH$_2$ unit of the pentenyl ligand, compared to those seen for free olefins.

As shown by the crystal structure discussed earlier, the ring formed by the pentenyl ligand in the Rh DBCOT complex **2** adopts a chair conformation (Figure 1). A 1D NOESY study shows that this conformation persists in solution: when the olefinic methine proton on the pentenyl chain is irradiated for 500 ms, a sizable NOE can be observed for the axial methyl resonance (SI Figure S3.10). If the pentenyl chain were to adopt a boat conformation, no NOE should be expected.

In the $^1$H NMR spectrum of **2**, the $J_{RhC}$ coupling constants to the olefinic DBCOT carbons that are cis to the alkyl group (16.5 and 11.4 Hz) are significantly larger (Table 2) than those to the olefinic DBCOT carbons that are trans to the alkyl (5.8 and 5.1 Hz). Similar differences in the $J_{RhC}$ coupling constants are also observed in the Rh COD complex **1** and the Rh NBD complex **3**. All these observations are consistent with the observation that the Rh−C bond distances to the olefinic DBCOT carbon atoms in **2** are different owing to the differing trans influence[11] abilities of the alkyl and olefin ends of the pentenyl ligand (see above).

Crabtree et al. has previously pointed out that DBCOT is a better $\pi$-acceptor than COD, and thus binds more strongly to rhodium and iridium.[10] A similar trend is observed here: the $J_{RhC}$ coupling constant to the olefinic diene carbon atoms decreases in the order of DBCOT > COD > NBD, indicating that the metal-diene bonding strength increases in the same order. Likewise, the $J_{RhC}$ coupling constant to the $\alpha$-CH$_2$ and olefinic carbon atoms of the pentenyl ligand increase in the order of **2** < **1** < **3** (Table 2), indicating that the dienes can be arranged on a trans influence series as DBCOT > COD > NBD.

Compound **5**, as isolated, contains ∼0.57 equiv of 4,4-dimethyl-1-pentene and traces of its isomer (*E*)-4,4-dimethyl-2-pentene. The $^1$H chemical shifts for the olefinic protons in 4,4-dimethyl-1-pentene ($\delta$ 5.62 for methine and 4.85 for methylene) in the presence of **5** are slightly shielded from those of pure 4,4-dimethyl-1-pentene ($\delta$ 5.79 for methine and 5.02 for methylene).[3,4] Because resonances due to only one organoiridium species are observed, the 4,4-dimethyl-1-pentene ligand must be rapidly associating and dissociating from **5** in solution.

**Olefin Decomplexation of the 2,2-Dimethlpent-4-en-1-yl Ligand.** We have previously shown that the C=C double bonds in Pt(CH$_2$CMe$_2$CH$_2$CH=CH$_2$)$_2$ are weakly coordinating, and decomplex reversibly from the Pt center at rates that are on the NMR time scale at room temperature.[3] The olefin decomplexation occurs by means of a "face-exchange" process[15,16] in which Pt becomes bound to the other face of the olefin; this same process causes the exchange of the axial and equatorial resonances of the pentenyl ring. The olefin face exchange (or "alkene flipping")[17] phenomenon is also observed for the Rh DBCOT complex **2**: when a solution of **1** in toluene-$d_8$ is warmed from room temperature, all the NMR resonances broaden except those for the terminal vinyl protons in the pentenyl ligand, which have no exchange partner (Figure 5).

Such olefin face exchange processes are also seen for the other M(CH$_2$CMe$_2$CH$_2$CH=CH$_2$)(diene) complexes, as indicated by the presence of cross peaks in the HSQC NMR spectra, and EXSY peaks in the NOESY spectra (see SI Section 3). Here, we will focus on the olefin decomplexation process in **2**, due to its well-defined composition and higher thermal stability.

We carried out the SST experiment betwThe rate of olefin face exchange in **2** was determined from simulations of the variable temperature $^1$H NMR line shapes of the diastereotopic methyl groups in the pentenyl ligand (note that the rate of

**Table 2. Selected $^1$H and $^{13}$C NMR Data for the $\eta^1$,$\eta^2$-2,2-Dimethylpent-4-en-1-yl Complexes of Rhodium and Iridium**

| | 1 | 2 | 3 | 4 | 5 |
|---|---|---|---|---|---|
| $^1$H $\delta$ ($\alpha$-CH$_2$) | 1.43, 1.11 | 1.79, 0.67 | 1.16, 0.80 | 1.94. 1.74 | 1.76, 1.43 |
| $^1$H $\delta$ (—CH=)[a] | 5.74 | 5.94 | 5.28 | 5.19 | 5.47 |
| $^1$H $\delta$ (=CH$_2$)[a] | 3.64, 3.50 | 3.73, 3.62 | 3.28, 3.30 | 3.50, 3.18 | 3.37, 3.31 |
| $^1$H $^3J_{HH}$ (olefinic)[a]/Hz | 16, 8.6 | 15.9, 8.6 | 15.8, 9.2 | 14.9, 8.9 | 14.0, 8.8 |
| $^{13}$C $\delta$ ($\alpha$-CH$_2$) | 60.13 | 65.22 | 63.46 | 63.41 | 68.33 |
| $^{13}$C $^1J_{RhC}$ ($\alpha$-CH$_2$)/Hz | 21.2 | 19.4 | 24.0 | | |
| $^{13}$C $\delta$ (—CH=) | 112.2 | 118.43 | 106.47 | 99.20 | 103.6 |
| $^{13}$C $\delta$ (=CH$_2$) | 86.03 | 93.11 | 80.41 | 77.93 | 83.75 |
| $^{13}$C $^1J_{RhC}$ (—CH=)/Hz | 7.9 | 7.3 | 8.0 | | |
| $^{13}$C $^1J_{RhC}$ (=CH$_2$)/Hz | 5.2 | 4.0 | 5.6 | | |
| $^{13}$C $\delta$ (diene CH)[b] | 85.20, 82.09 | 84.89, 82.70 | 66.28, 64.13 | 75.86, 74.99 | 79.48, 77.20 |
| $^{13}$C $\delta$ (diene CH)[c] | 91.37, 86.03 | 96.31, 93.31 | 77.69, 72.59 | 76.60, 73.11 | 75.28, 72.88 |
| $^{13}$C $^1J_{RhC}$ (diene CH)/Hz[b] | 14.8, 11.1 | 16.5, 11.4 | 12.7, 9.9 | | |
| $^{13}$C $^1J_{RhC}$ (diene CH)/Hz[c] | 5.5, 5.2 | 5.8, 5.1 | 5.7, 4.8 | | |

[a]In pentenyl group. [b]cis to alkyl. [c]trans to alkyl.


https://dx.doi.org/10.1021/acs.organomet.0c00798
Organometallics 2021, 40, 714−724

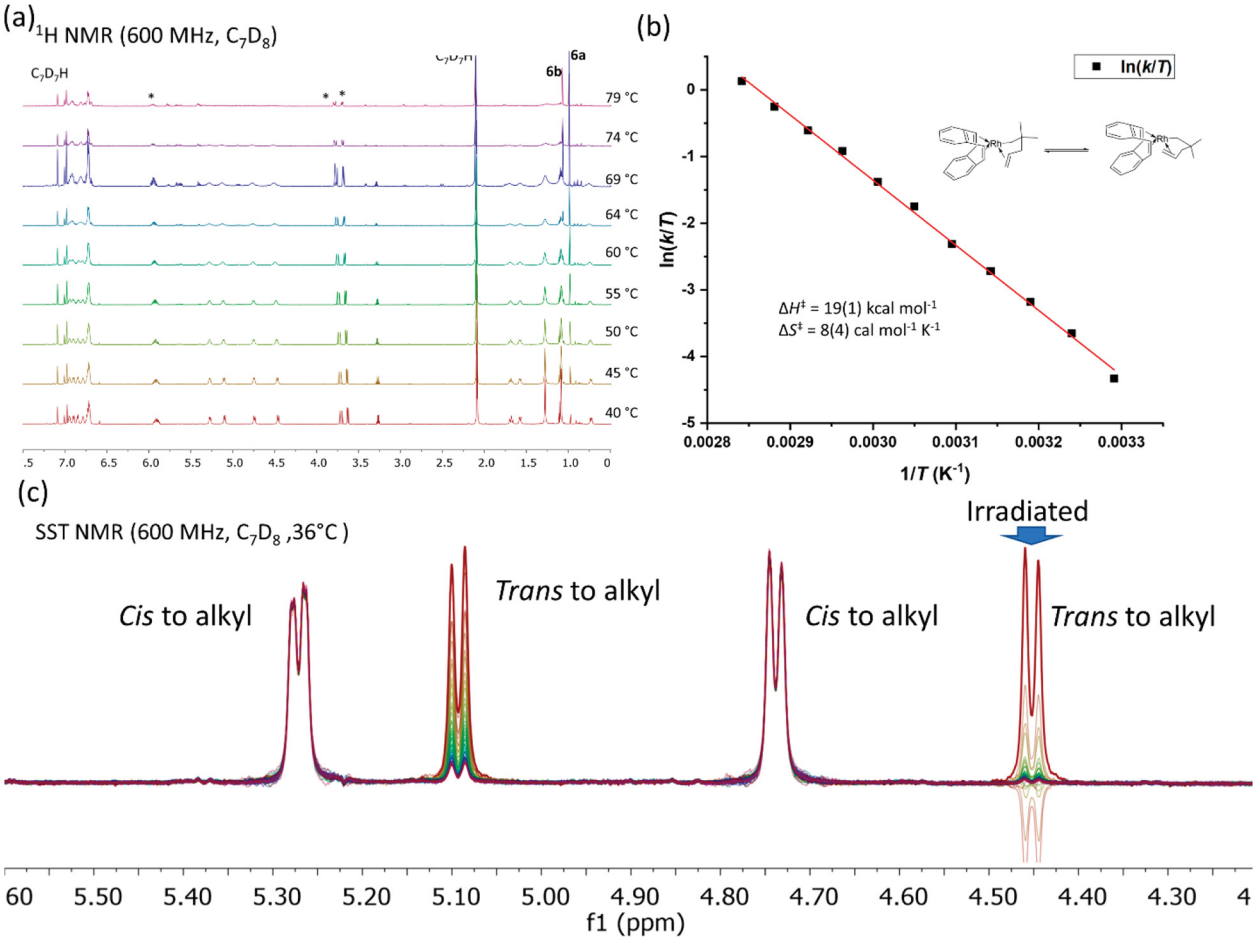


**Figure 5.** (a) VT-$^1$H NMR spectrum of **2** in toluene-$d_8$. All resonances except the vinyl resonances on the pentenyl chain (labeled with "*") are broadened due to exchange. Allylrhodium species **6a** and **6b** are formed at higher temperatures. (b) Eyring plot of the rate of olefin decomplexation of **2** in toluene-$d_8$; (c) Superimposed spectra of the DBCOT resonance of **2** as a function of presaturation time. The spectra were collected with presaturation times that increased in increments of 0.02 s, with the longest presaturation time being 1 s.

olefin decomplexation is twice the rate of methyl exchange). A fit of 11 rates between 31 and 79 °C to the Eyring equation gives activation parameters of $\Delta H^{\ddagger}$ = 19 ± 1 kcal mol$^{-1}$ and $\Delta S^{\ddagger}$ = 8 ± 4 cal mol$^{-1}$·K$^{-1}$ for olefin decomplexation (Figure 5). These activation paramaters are almost identical to those of $\Delta H^{\ddagger}$ = 19 ± 1 kcal mol$^{-1}$ and $\Delta S^{\ddagger}$ = 10 ± 3 cal mol$^{-1}$·K$^{-1}$ seen for Pt($CH_2CMe_2CH_2CH{=}CH_2$)$_2$.[3] The positive entropy of activation is consistent with a mechanism in which the metal-olefin bond is broken without concomitant association of solvent molecules.[18,19] As we have discussed elsewhere,[3] the resulting intermediate is either a three-coordinate 14 e$^-$ species (if the olefin simply dissociates)[7,20,21] or a four-coordinate 16 e$^-$ C−H $\sigma$-complex (if the metal-olefin bond is broken but replaced with an agostic interaction).[17,22,23] To distinguish these mechanisms, we carried out a spin saturation transfer (SST) experiment involving the olefinic DBCOT resonances of **2**. As we showed above, all four olefinic protons on DBCOT in **2** have unique chemical shifts in the room temperature $^1$H NMR spectrum. If the vinyl group on the pentenyl ligand completely dissociates to form a true three-coordinate Rh$^I$ complex,[24] and if this intermediate is either Y-shaped, or T-shaped but the Y-shape is energetically accessible, then all four DBCOT olefinic DBCOT resonances should exchange with one another at a rate comparable to the rate of olefin decomplexation.een 10 and 40 °C; higher temperatures were not possible because **2** starts to decompose rapidly above 40 °C. Upon irradiation of an olefinic DBCOT resonance trans to the alkyl group ($\delta \sim 4.5$), only the other DBCOT resonance trans to the alkyl group shows a decrease in intensity due to SST. The intensities of the resonance cis to the alkyl group show no change within experimental error (Figure 5). In addition, the measured rates from the SST experiment were in reasonable agreement with those obtained from line shape fitting (Table 3), after taking into account the effect of nuclear Overhauser effects (NOEs) on the intensities seen in the SST study, and the relatively large error in rates determined by line shape analysis when the exchange rate is slow.

This result suggests that pentenyl ligands undergo face exchange/alkene flipping by means of an intermediate in which the M-alkene interaction decomplexes but is replaced with an

**Table 3. Temperature-Dependent Rate of "Alkene Flipping" in 2 in Toluene-$d_8$**

| T/ °C | Exchange rate (SST) /s$^{-1}$ | Exchange rate (line shape) /s$^{-1}$ |
|---|---|---|
| 11 | 0.93 | |
| 21 | 1.7 | |
| 31 | 3.2 | 2.0 |
| 36 | 4.5 | 4.0 |
| 40 | 6.2 | 6.5 |


https://dx.doi.org/10.1021/acs.organomet.0c00798
Organometallics 2021, 40, 714−724

agostic interaction in a concerted fashion. If a three-coordinate intermediate is formed, it must have a T-shape and be stereochemically rigid; that is, unable to convert into a Y shape.[25,26] Olefin decomplexation in $Pt(CH_2CMe_2CH_2CH{=}CH_2)_2$ presumably follows a similar mechanism (Scheme 2).[3]

**Scheme 2. Possible Mechanism for Olefin Decomplexation of 2 in $C_7D_8$**

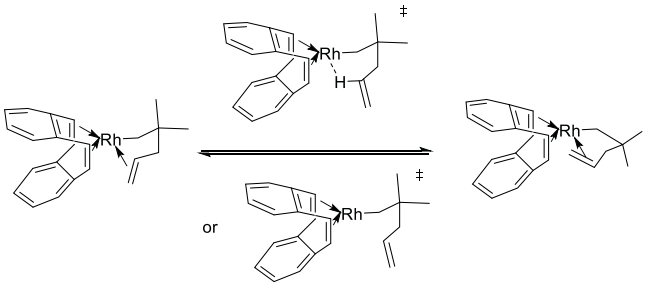


The mechanism of olefin decomplexation in **2** is different from that seen in $(C_5R_5)_2Zr(OCMe_2CH_2CH_2CH{=}CH_2)^+$ and analogous complexes, in which the olefin decomplexation is accompanied by migration of the $\eta^1$-ligand to the vacant coordination site.[15,16]

**Thermolysis of 2 in Solution.** When a solution of **2** is gradually warmed from room temperature to 80 °C over ~4 h, it slowly isomerizes and generates two new soluble organorhodium species (Figure 6). Unlike $Pt(CH_2CMe_2CH_2CH{=}CH_2)_2$, which generates a large amount of black solid when heated,[4] for **2**, no solid is formed.

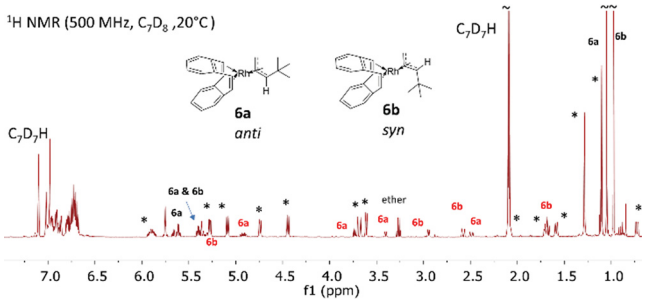


**Figure 6.** $^1$H NMR spectrum of the products of the thermolysis of **2**. The resonances of **2** are labeled with asterisks, and the resonances of the allyl protons of **6a** and **6b** are highlighted in red.

The two new rhodium complexes, $Rh(\eta^3\text{-}anti\text{-}CH_2{=}CHCHCMe_3)(DBCOT)$ (**6a**) and $Rh(\eta^3\text{-}syn\text{-}CH_2{=}CHCHCMe_3)(DBCOT)$ (**6b**), contain *tert*-butylallyl groups; these groups are probably formed by oxidative addition of the allylic C−H bond in **2** to form a rhodium(III) allyl hydride intermediate, followed by reductive elimination of the hydride ligand with the $\alpha$-$CH_2$ carbon. Of the two compounds, **6a** is initially formed, whereas **6b** becomes the major product at longer times and higher temperatures. Thus, **6a** is the kinetic product and **6b** is the thermodynamic product of the isomerization; **6b** is more stable thermodynamically because it is less sterically crowded. Most likely the isomerization involves an $\eta^3$-$\eta^1$-$\eta^3$ mechanism.[27−29]

In the solid-state structure of **2**, both $\gamma$-$CH_2$ protons are pointing away from metal center and they cannot participate in C−H activation in this conformation. The formation of **6a** as the kinetic product suggests that the pentenyl chain twists to a boat conformation before C−H activation occurs (Scheme 3).

**Scheme 3. Decomposition Mechanism of 2 in $C_7D_8$**

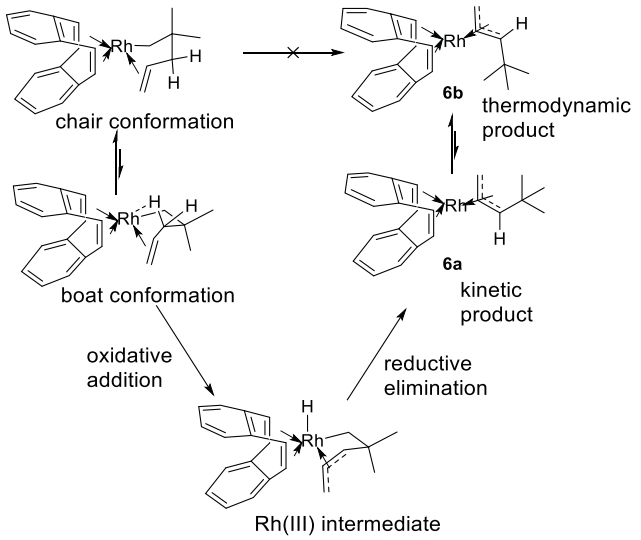


The thermolysis of **2** differs from that of the related platinum(II) compound $Pt(CH_2CMe_2CH_2CH{=}CH_2)_2$[4] in two principal ways. First, thermolysis of **2** is much faster than that of $Pt(CH_2CMe_2CH_2CH{=}CH_2)_2$: ~ 30% of **2** decomposes within 3 h at 80 °C, whereas ~30% of $Pt(CH_2CMe_2CH_2CH{=}CH_2)_2$ decomposes only after 12 days of heating at 90 °C. Second, thermolysis of **2** occurs exclusively by activating an allylic (i.e., $\gamma$) C−H bond, whereas both allylic and olefinic C−H bonds are activated during the thermolysis of $Pt(CH_2CMe_2CH_2CH{=}CH_2)_2$.[4] One possibility is that, in **2**, there is a low barrier for formation of the $\sigma$-complex of the $\gamma$-C−H bond, so that the rate limiting step is not the formation of the $\sigma$-complex, as it is in $Pt(CH_2CMe_2CH_2CH{=}CH_2)_2$,[4] but instead is the oxidative addition step. If this is the case, then the weakest[30] C−H bond in **2** will be selectively activated. Alternatively, the differences between **2** and $Pt(CH_2CMe_2CH_2CH{=}CH_2)_2$ may reflect electronic factors involving the energies and spatial distributions of the valence orbitals that the metal uses in the C−H bond activation processes, or the differences may reflect interligand steric factors that affect the energy required for the pentenyl chain to twist into the boat conformation necessary for allylic C−H activation to occur.

**Concluding Remarks.** We have made three new four-coordinate rhodium(I) complexes of stoichiometry $Rh(\eta^1,\eta^2$-2,2-dimethylpent-4-en-1-yl)(diene), where diene = 1,5-cyclooctadiene (COD, **1**), dibenzo[a,e]cyclooctatetraene (DBCOT, **2**), or norbornadiene (NBD, **3**), as well as the analogous iridium complexes with COD (**4**) and DBCOT (**5**), although, as isolated, the latter contained 0.57 equiv of bound 4,4-dimethyl-1-pentene. Also isolated was the adduct of the iridium DBCOT complex with 4,4,7,7-tetramethyldeca-1,9-diene (**5′**). In all these compounds, the pentenyl ligand chelates to the metal center by means of a sigma-alkyl bond at one end of the chain, and a pi-olefin bond at the other.

The C=C bonds of the pentenyl ligand in compounds **1**−**4** (and presumably in **5** also) are weakly coordinating and reversibly decomplex in solution on the NMR time scale. Activation parameters of $\Delta H^{\ddagger}$ = 19 ± 1 kcal mol$^{-1}$ and $\Delta S^{\ddagger}$ =


https://dx.doi.org/10.1021/acs.organomet.0c00798
Organometallics 2021, 40, 714−724

8 ± 4 cal $mol^{-1}·K^{-1}$ for olefin decomplexation were measured for **2**. SST studies show that the olefin decomplexation in **2** does not involve the formation of a Y-shaped three-coordinate intermediate. Overall, the olefin decomplexation of **2** most likely occurs by means of a C−H $\sigma$-complex, or, less likely, a T-shaped intermediate which is too short-lived for the alkyl group to migrate to the vacant coordination site.

When heated, **1** decomposes to form the allylic compounds Rh($\eta^3$-*anti*-$CH_2$=CHCHCMe$_3$)(DBCOT) (**6a**) and Rh($\eta^3$-*syn*-$CH_2$=CHCHCMe$_3$)(DBCOT) (**6b**). The decomposition occurs by activation of an allylic C−H bond to form a $Rh^{III}$ allyl hydride species. Subsequent reductive elimination of the hydride ligand with the $\alpha$-$CH_2$ carbon generates **6a**, which then isomerizes by a $\eta^3$-$\eta^1$-$\eta^3$ mechanism to form the more thermodynamically stable isomer **6b**.

## EXPERIMENTAL SECTION

All experiments were carried out in vacuum or under argon using standard Schlenk techniques. Solvents (pentane, diethyl ether, THF) were distilled under nitrogen from sodium/benzophenone immediately before use. 4-Bis(trimethylsilyl)benzene (Sigma-Aldrich) was obtained from commercial sources. Benzene-$d_6$ and toluene-$d_8$ (Cambridge Isotope Laboratories) were distilled under argon from sodium/benzophenone. The compounds $[RhCl(COD)]_2$,[31] $[RhCl(NBD)]_2$,[32] $[RhCl(DBCOT)]_2$,[33] $[IrCl(COD)]_2$,[34] $[IrCl(DBCOT)]_2$,[33] (2,2-dimethylpent-4-en-1-yl)magnesium bromide,[3] and (2,2-dimethylpent-4-en-1-yl)lithium[9] were prepared by literature procedures.

Melting points were determined on a Thomas-Hoover Uni-Melt apparatus in sealed capillaries under argon. The $^1$H and $^{13}$C NMR data were recorded on a Bruker Avance III HD spectrometer equipped with a 5 mm BBFO CryoProbe at 11.74 T. Chemical shifts are reported in $\delta$ units (positive shifts to higher frequency) relative to TMS ($^1$H, $^{13}$C). X-ray crystallographic data were collected by the staff of the G. L. Clark X-ray Laboratory at the University of Illinois. Microanalyses were performed by the University of Illinois Microanalytical Laboratory. For some samples, it was necessary to add a combustion aid (a mixture of silver vanadate, silver tungstate, and cobaltic oxide) to avoid incomplete combustion.

**(1,5-Cyclooctadiene)($\eta^1$,$\eta^2$-2,2-dimethylpent-4-en-1-yl)rhodium(I), (1).** To a solution of $[RhCl(COD)]_2$ (34 mg, 0.069 mmol) in THF (10 mL) at −80 °C was added a solution of (2,2-dimethylpent-4-en-1-yl)lithium (16 mg, 0.15 mmol) in pentane (5 mL). The mixture was warmed to −20 °C and was stirred this temperature for 1 h, over which time the solution color changed from yellow to orange. The pentane was removed under vacuum at −20 °C, the cooling bath was removed, and THF was removed under vacuum rapidly enough that the sample remained cold. The resulting dark oil was cooled to −80 °C, and extracted with pentane (10 mL). The extract was filtered and evaporated to dryness to give the product as an orange oil. Yield (measured by NMR using 1,4-bis(trimethylsilyl)benzene as an integration standard): 13 mg (31%). Satisfactory microanalytical data could not be obtained owing to the low melting point and sensitivity of the compound toward air, water and heat. MS (EI, $m/e$). Calcd for $C_{15}H_{25}Rh$: 308.3. Found: 308.3. $^1$H NMR (500 MHz, $C_6D_6$, 20 °C): $\delta$ 5.74 (m, 1 H, —CH=), 4.77 (m, 1 H, CH of COD), 4.39 (m, 1 H, CH of COD), 4.09 (m, 1 H, CH(COD)), 3.64 (d, 1 H, $^3J_{HH}$ = 8.6 Hz, $^2J_{HH}$ = 1.5 Hz, =$CH_2$), 3.50 (m, 1 H, CH of COD), 3.50 (d, 1 H, $^3J_{HH}$ = 16 Hz, =$CH_2$), 2.30−2.20 (m, 2 H, $CH_2$ of COD cis to —CH=$CH_2$ and equatorial $\gamma$-$CH_2$), 2.13−1.92 (m, 4 H, $CH_2$ of COD), 1.88 (m, 1 H, $CH_2$ of COD trans to −CH=$CH_2$), 1.78 (m, 2 H, $CH_2$ of COD cis to —CH=$CH_2$), 1.73 (dd, 1 H, $^2J_{HH}$ ∼ $^3J_{HH}$ ∼ 11 Hz, 1H, $\gamma$-$CH_2$, axial), 1.43 (d, $^2J_{HH}$ = 10.3 Hz, 1H, axial Rh-$CH_2$), 1.39 (s, 3H, axial $\beta$-Me), 1.20 (s, 3 H, equatorial $\beta$-Me), 1.11 (dd, $^2J_{HH}$ = 10.3 Hz, $^4J_{HH}$ = 3.0 Hz, 1 H, equatorial Rh-$CH_2$). $^{13}$C{$^1$H} NMR (126 MHz, $C_6D_6$, 20 °C): $\delta$ 112.20 (d, $J_{RhC}$ = 7.9 Hz, —CH=), 93.26 (d, $J_{RhC}$ = 5.6 Hz, CH of COD cis to —CH=$CH_2$), 91.37 (d, $J_{RhC}$ = 5.5 Hz, CH of COD cis to —CH=$CH_2$), 86.03 (d, $J_{RhC}$ = 5.2 Hz, =$CH_2$), 85.20 (d, $J_{RhC}$ = 14.8 Hz, CH of COD trans to —CH=$CH_2$), 82.09 (d, $J_{RhC}$ = 11.1 Hz, −CH of COD trans to CH=$CH_2$), 60.13 (d, $J_{RhC}$ = 21.2 Hz, Rh−$CH_2$), 53.03 (d, $J_{RhC}$ = 2.0 Hz, $\beta$-C), 51.11 (d, $J_{RhC}$ = 1.1 Hz, $\gamma$-$CH_2$), 33.90 (d, $J_{RhC}$ = 1.0 Hz, $CH_2$ of COD trans to —CH=$CH_2$), 34.29 (d, $J_{RhC}$ = 1.3 Hz, equatorial $\beta$-Me), 31.16 (s, $CH_2$ of COD cis to —CH=$CH_2$), 30.82 (s, axial $\beta$-Me), 30.45 (s, $CH_2$ of COD trans to —CH=$CH_2$), 29.90 (s, $CH_2$ of COD cis to —CH=$CH_2$).

**(Dibenzo[*a*,*e*]cyclooctatetraene)($\eta^1$,$\eta^2$-2,2-dimethylpent-4-en-1-yl)rhodium(I), (2).** To a suspension of $[RhCl(DBCOT)]_2$ (260 mg, 0.75 mmol) in THF (20 mL) at −80 °C was added a solution of (2,2-dimethylpent-4-en-1-yl)lithium (94 mg, 0.91 mmol) in pentane (5 mL). The mixture was stirred for 30 min at −80 °C, then warmed to −20 °C and was stirred this temperature for 4 h. The pentane was removed under vacuum at −20 °C, and the THF was removed at 0 °C. The residue was extracted with pentane (4 × 40 mL), and the extracts were filtered, combined, and evaporated to dryness. The resulting orange solid was dissolved in diethyl ether (50 mL), and the resulting solution was concentrated to ∼5 mL and kept at −20 °C to afford the product as orange crystals. Yield: 0.123 g (40%). Anal. Calcd for $C_{23}H_{25}Rh$: C, 68.3; H, 6.23. Found: C, 68.0; H, 6.40. Mp. 145−147 °C (dec). $^1$H NMR (500 MHz, $C_6D_6$, 20 °C): $\delta$ 7.02 (m, 1 H, aromatic CH), 6.96 (d, 1 H, $^3J_{HH}$ = 6.9 Hz, aromatic CH), 6.92 (d, 1 H, $^3J_{HH}$ = 7.0 Hz, aromatic CH), 6.86 (m, 1 H, aromatic CH), 6.82−6.72 (m, 4 H, aromatic CH), 5.94 (m, 1 H, —CH=), 5.34 (dd, $^3J_{HH}$ = 8.1 Hz, $J_{RhH}$ = 2.6 Hz, 1 H, =CH— of DBCOT, cis to alkyl), 5.12 (d, $^3J_{HH}$ = 8.9 Hz, 1 H, =CH— of DBCOT, trans to alkyl), 4.82 (d, $^3J_{HH}$ = 7.8 Hz, 1 H, =CH— of DBCOT, cis to alkyl), 4.48 (d, $^3J_{HH}$ = 8.9 Hz, 1 H, =CH— of DBCOT, trans to alkyl), 3.73 (d, 1 H, $^3J_{HH}$ = 15.9 Hz, =$CH_2$), 3.62 (d, 1 H, $^3J_{HH}$ = 8.6 Hz, $J_{RhH}$ = 1.4 Hz, =$CH_2$), 2.12 (m, 1 H, equatorial $\gamma$-$CH_2$), 1.72 (dd, 1 H, $^2J_{HH}$ ∼ $^3J_{HH}$ ∼ 11 Hz, 1H, axial $\gamma$-$CH_2$), 1.67 (d, $^2J_{HH}$ = 10.2 Hz, 1H, axial Rh-$CH_2$), 1.33 (s, 3H, axial $\beta$-Me), 1.14 (s, 3 H, equatorial $\beta$-Me), 0.79 (dd, $^2J_{HH}$ = 10.2 Hz, $^4J_{HH}$ = 2.8 Hz, 1 H, equatorial Rh-$CH_2$). $^{13}$C{$^1$H} NMR (126 MHz, $C_6D_6$, 20 °C): $\delta$ 145.83 (d, $J_{RhH}$ = 1.6 Hz, ipso-C), 145.26 (s, ipso-C), 144.24 (s, ipso-C), 144.04 (s, ipso-C), 126.21 (s, aromatic CH), 126.17 (s, aromatic CH), 126.12 (s, aromatic CH), 126.09 (s, aromatic CH), 125.98 (s, aromatic CH), 125.90 (s, aromatic CH), 125.81 (s, aromatic CH), 125.69 (d, $J_{RhH}$ = 2.6 Hz, aromatic CH), 118.43 (d, $J_{RhC}$ = 7.3 Hz, —CH=), 96.31 (d, $J_{RhC}$ = 5.8 Hz, =CH— of DBCOT cis to —CH=$CH_2$), 93.31 (d, $J_{RhC}$ = 5.1 Hz, =CH— of DBCOT cis to —CH=$CH_2$), 93.11 (d, $J_{RhC}$ = 4.0 Hz, =$CH_2$), 84.89 (d, $J_{RhC}$ = 16.5 Hz, =CH— of DBCOT trans to —CH=$CH_2$), 82.70 (d, $J_{RhC}$ = 11.4 Hz, =CH— of DBCOT trans to CH=$CH_2$), 65.22 (d, $J_{RhC}$ = 19.4 Hz, Rh−$CH_2$), 53.89 (d, $J_{RhC}$ = 2.1 Hz, $\beta$-C), 50.54 (s, $\gamma$-$CH_2$), 32.99 (d, $J_{RhC}$ = 1.3 Hz, equatorial $\beta$-Me), 30.72 (s, axial $\beta$-Me).

**(Bicyclo[2.2.1]hepta-2,5-diene)($\eta^1$,$\eta^2$-2,2-dimethylpent-4-en-1-yl)rhodium(I), (3).** This compound was prepared from $[RhCl(NBD)]_2$ (0.022 g, 0.096 mmol) according to the procedure for synthesizing **2**. The product was obtained as an orange oil. Yield (measured by NMR using 1,4-bis(trimethylsilyl)benzene as an integration standard): 9.6 mg (34%). Satisfactory microanalytical data could not be obtained owing to the low melting point and sensitivity of the compound toward air, water and heat. $^1$H NMR (500 MHz, $C_6D_6$, 20 °C): $\delta$ 5.28 (m, 1 H, —CH=), 4.57 ("q", "$J$" = 4 Hz, 1 H, =CH— of NBD, cis to alkyl), 4.13 (m, 1 H, =CH— of NBD, trans to alkyl), 4.06 ("q", "$J$" = 2 Hz, 1 H, =CH— of NBD, cis to alkyl), 3.99 (s with a shoulder, 1 H, =CH— of NBD, trans to alkyl), 3.60 (br s, 1 H, bridge head CH of NBD), 3.28 (d, 1 H, $^3J_{HH}$ = 9.2 Hz, =$CH_2$), 3.26 (br s, 1 H, bridge head CH of NBD), 3.03 (d, 1 H, $^3J_{HH}$ = 15.8 Hz, =$CH_2$), 2.47 (m, 2 H, equatorial $\gamma$-$CH_2$), 1.58 (dd, 1 H, $^2J_{HH}$ ∼ $^3J_{HH}$ ∼ 11.7 Hz, 1H, axial $\gamma$-$CH_2$), 1.46 (dt, 1 H, $^2J_{HH}$ = 7.8 Hz, $^3J_{HH}$ = 1.5 Hz, $CH_2$ of NBD), 1.39 (s, 3H, axial $\beta$-Me), 1.35 (dt, 1 H, $^2J_{HH}$ = 7.8 Hz, $^3J_{HH}$ = 1.3 Hz, $CH_2$ of NBD), 1.21 (s, 3 H, equatorial $\beta$-Me), 1.16 (d, $^2J_{HH}$ = 11.5 Hz, 1H, axial Rh-$CH_2$), 0.80 (dd, $^2J_{HH}$ = 11.2 Hz, $^4J_{HH}$ = 2.2 Hz, 1 H, equatorial Rh-$CH_2$).$^{13}$C{$^1$H} NMR (126 MHz, $C_6D_6$, 20 °C): $\delta$ 106.47 (d, $J_{RhC}$ = 8.0 Hz, —CH=), 80.41 (d, $J_{RhC}$ = 5.6 Hz, =$CH_2$), 77.69 (d, $J_{RhC}$ = 5.7 Hz, CH


https://dx.doi.org/10.1021/acs.organomet.0c00798
Organometallics 2021, 40, 714−724

of NBD cis to —CH=$CH_2$), 72.59 (d, $J_{RhC}$ = 4.8 Hz, CH of NBD cis to —CH=$CH_2$), 69.56 (d, $J_{RhC}$ = 12.7 Hz, CH of NBD trans to —CH=$CH_2$), 66.28 (d, $J_{RhC}$ = 4.4 Hz, $CH_2$ of NBD), 64.13 (d, $J_{RhC}$ = 9.9 Hz, — CH of NBD trans to —CH=$CH_2$), 63.46 (d, $J_{RhC}$ = 24.0 Hz, Rh–$CH_2$), 55.18 (d, $J_{RhC}$ = 1.1 Hz, $\beta$-C), 52.96 (s, bridge head CH of NBD), 51.31 (d, $J_{RhC}$ = 0.8 Hz, $\gamma$-$CH_2$), 50.35 (d, $J_{RhC}$ = 2.6 Hz, bridge head CH of NBD), 33.38 (s, equatorial $\beta$-Me), 30.30 (s, axial $\beta$-Me).

**(1,5-Cyclooctadiene)($\eta^1$,$\eta^2$-2,2-dimethylpent-4-en-1-yl)-iridium(I), (4).** To a solution of $[IrCl(COD)]_2$ (0.033 g, 0.049 mmol) in THF (10 mL) at −80 °C was added dropwise a solution of (2,2-dimethylpent-4-en-1-yl)lithium (0.012 g, 0.049 mmol) in pentane (5 mL). The mixture was stirred at −80 °C for 30 min and warmed to −20 °C for 3 h, over which time the solution color changed from yellow to red. The pentane was removed under vacuum at −20 °C, and the THF was removed under vacuum at room temperature. The resulting dark oil was extracted with pentane (10 mL). The extract was filtered and evaporated to dryness to give the product as a red-orange oil. Yield (measured by NMR using 1,4-bis(trimethylsilyl)benzene as an integration standard): 24 mg (61%). Mp. < −10 °C. Satisfactory microanalytical data could not be obtained owing to the low melting point and sensitivity of the compound toward air, water and heat. HRMS (EI, $m/e$). Calcd for $C_{15}H_{25}Ir$: 398.15853. Found: 398.15781. $^1$H NMR (400 MHz, $C_6D_6$, 20 °C): $\delta$ 5.19 (m, 1 H, —CH=), 4.29 (m, 1 H, CH of COD trans to CH=$CH_2$), 4.06 (m, 1 H, CH of COD trans to CH=$CH_2$), 3.78 (m, 1 H, CH of COD cis to CH=$CH_2$), 3.50 (d, 1 H, $^3J_{HH}$ = 8.9 Hz, =$CH_2$), 3.18 (d, 1 H, $^3J_{HH}$ = 14.9 Hz, =$CH_2$), 3.00 (m, 1 H, CH of COD cis to —CH=$CH_2$), 2.54 (ddd, $^2J_{HH}$ = 11.8 Hz, $^3J_{HH}$ = 4.5 Hz, $^4J_{HH}$ = 2.6 Hz, 1 H, equatorial $\gamma$-$CH_2$), 1.57–2.15 (m, 8 H, $CH_2$ of COD), 1.94 (dd, $^2J_{HH}$ = 12.6 Hz,$^4J_{HH}$ = 2.6 Hz, 1 H, equatorial Ir-$CH_2$), 1.74 (d, $^2J_{HH}$ = 12.4 Hz, 1H, axial Ir-$CH_2$), 1.61 (dd, $^2J_{HH}$ = 11.3 Hz, $^3J_{HH}$ = 11.3 Hz, 1 H, axial $\gamma$-$CH_2$), 1.29 (s, 3 H, $\beta$-Me), 1.33 (s, 3 H, $\beta$-Me). $^{13}C\{^1H\}$ NMR (101 MHz, $C_6D_6$, 20 °C): $\delta$ 99.20 (s, —CH=), 77.93 (s, =$CH_2$), 76.60 (s, CH of COD cis to —CH=$CH_2$), 75.86 (s, CH of COD trans to —CH=$CH_2$), 74.99 (s, CH of COD trans to —CH=$CH_2$), 73.11 (s, —CH of COD cis to CH=$CH_2$), 63.41 (s, Ir–$CH_2$), 55.47 (s, $\beta$-C), 52.93 (s, $\gamma$-$CH_2$), 34.29 (s, $\beta$-Me), 32.44 (s, $CH_2$ of COD trans to —CH=$CH_2$), 32.24 (s, $CH_2$ of COD cis to —CH=$CH_2$), 31.96 (s, $CH_2$ of COD trans to —CH=$CH_2$), 30.31 (s, $\beta$-Me), 30.20 (s, $CH_2$ of COD cis to —CH=$CH_2$).

**(Dibenzo[*a*,*e*]cyclooctatetraene)($\eta^1$,$\eta^2$-2,2-dimethylpent-4-en-1-yl)iridium(I)·0.57(4,4-dimethyl-1-pentene), (5).** To a suspension of $[IrCl(DBCOT)]_2$ (0.161 g, 0.37 mmol) in pentane (20 mL) at 20 °C was added a solution of (2,2-dimethylpent-4-en-1-yl) lithium (43 mg, 0.40 mmol) in pentane (5 mL). The mixture was stirred for 48 h at 20 °C, then filtered to give a red solution. The pentane was removed under vacuum at 20 °C to give a mixture of brown and white solids. Yield: 45 mg (11%). Anal. Calcd for $C_{23}H_{25}Ir{\cdot}0.57C_7H_{14}$: C, 59.0; H, 6.05. Found: C, 58.9; H, 6.08. HRMS (EI, $m/e$). Calcd for $C_{23}H_{25}Ir$: 494.15875. Found: 494.15853. $^1$H NMR (500 MHz, $C_6D_6$, 20 °C) for **5**: $\delta$ 6.98 (m, 3 H, aromatic CH), 6.89 (m, 1 H, aromatic CH), 6.78–6.67 (m, 4 H, aromatic CH), 5.47 (m, 1 H, —CH=), 4.99 (d, $^3J_{HH}$ = 7.9 Hz, 1 H, =CH— of DBCOT), 4.91 (d, $^3J_{HH}$ = 7.9 Hz, 1 H, =CH— of DBCOT), 4.89 (d, $^3J_{HH}$ = 8.3 Hz, 1 H, =CH— of DBCOT), 3.92 (d, $^3J_{HH}$ = 8.3 Hz, 1 H, = CH– of DBCOT, trans to alkyl), 3.37 (d, $^3J_{HH}$ = 8.8 Hz, 1 H, =$CH_2$), 3.31 (d, $^3J_{HH}$ = 14.0 Hz, 1 H, =$CH_2$), 2.38 (ddd, $^2J_{HH}$ = 11.9 Hz, $^3J_{HH}$ = 4.6 Hz, $^4J_{HH}$ = 2.4 Hz, 1 H, equatorial $\gamma$-$CH_2$), 1.76 (d, $^2J_{HH}$ = 12.5 Hz, 1 H, axial Ir-$CH_2$), 1.66 (dd, $^2J_{HH} \sim {}^3J_{HH} \sim$ 11 Hz, 1H, axial $\gamma$-$CH_2$), 1.43 (dd, $^2J_{HH}$ = 12.5 Hz, $^4J_{HH}$ = 2.4 Hz, 1 H, equatorial Ir-$CH_2$), 1.24 (s, 3 H, axial $\beta$-Me), 1.22 (s, 3 H, equatorial $\beta$-Me). $^{13}C\{^1H\}$ NMR (126 MHz, $C_6D_6$, 20 °C) for **5**: $\delta$ 146.07 (s, ipso-C), 145.80 (s, ipso-C), 145.78 (s, ipso-C), 126.21 (s, aromatic CH), 126.17 (s, aromatic CH), 126.04 (s, aromatic CH), 126.01 (s, aromatic CH), 125.87 (s, aromatic CH), 125.83 (s, aromatic CH), 125.62 (s, aromatic CH), 125.60 (s, aromatic CH), 103.6 (br, pentenyl —CH=), 83.75 (br, =$CH_2$), 79.48 (s, =CH— of DBCOT), 77.20 (s, =CH— of DBCOT), 75.28 (s, = CH— of DBCOT), 72.88 (s, =CH— of DBCOT), 68.33 (br, Ir–$CH_2$), 55.86 (s, $\beta$-C), 51.81 (s, $\gamma$-$CH_2$), 34.10 (s, equatorial $\beta$-Me), 30.44 (s, axial $\beta$-Me). Also present in the spectrum are resonances due to ∼0.5 equiv of unbound 4,4-dimethyl-1-pentene and ∼0.07 equiv of unbound 4,4-dimethyl-2-pentene: $^1$H NMR (500 MHz, $C_6D_6$, 20 °C) for 4,4-dimethyl-1-pentene: $\delta$ 5.62 (m, 1 H, —CH=), 4.81–4.89 (m, 2 H, =$CH_2$), 1.88 (d, 2 H, allylic $CH_2$), 0.86 (s, 9H, Me). $^1$H NMR (500 MHz, $C_6D_6$, 20 °C) for 4,4-dimethyl-2-pentene: $\delta$ 5.32 (dq, $^3J_{HH}$ = 15.5 Hz, 6.3 Hz, 2 H, =CH—), 1.60 (dd, $^3J_{HH}$ = 6.3 Hz, $^4J_{HH}$ = 1.5 Hz, 3 H, allylic Me), 1.00 (s, 9H, Me); one of the olefinic CH resonances overlaps with a resonance due to **5**.

**(Dibenzo[*a*,*e*]cyclooctatetraene)($\eta^1$,$\eta^2$-2,2-dimethylpent-4-en-1-yl)iridium(I)·0.5(4,4,7,7-tetramethyldeca-1,9-diene), (5′).** To a suspension of $[IrCl(DBCOT)]_2$ (0.20 g, 0.41 mmol) in diethyl ether (20 mL) at −80 °C was added a solution of (2,2-dimethylpent-4-en-1-yl)magnesium bromide (1.2 mL of a 0.36 M solution in diethyl ether, 0.43 mmol). The mixture was warmed to 20 °C and stirred for 48 h. The solvent was evaporated, and the residue was extracted with pentane (2 × 10 mL). The extracts were combined, quenched by addition of 1 drop of water, and dried over $MgSO_4$ for 12 h. The dark red pentane solution was filtered, the solvent was removed under vacuum, and the red residue was recrystallized from diethyl ether (ca. 1 mL) at −20 °C to give colorless crystals, which were characterized crystallographically. The crystals melt at room temperature and turn into a red oil, due to decomposition to form **5** and free 4,4,7,7-tetramethyldeca-1,9-diene.

**X-ray Crystallographic Analysis.** The following details were common to all of the crystal structure determinations; for details about individual compounds, see the SI. Crystals mounted on glass fibers with Krytox oil were transferred onto the diffractometer and kept at −173 °C in a cold nitrogen gas stream. Intensity data were collected on Bruker Apex II diffractometer equipped with a CCD detector or Bruker D8 Venture kappa diffractometer equipped with a Photon 100 CMOS detector. An I$\mu$s microfocus source provided the Mo K$\alpha$ radiation ($\lambda$ = 0.71073 Å) that was monochromated with multilayer mirrors. Standard peak search and indexing procedures gave rough cell dimensions. The collection, cell refinement and integration of intensity data were carried out with the APEX3 software.[35] The measured intensities were reduced to structure factor amplitudes and their estimated standard deviations by correction for background, scan speed, and Lorentz and polarization effects. No corrections for crystal decay were necessary. Systematically absent reflections were deleted and symmetry equivalent reflections were averaged to yield the set of unique data.

The initial model was obtained by direct methods (SHELXS),[36] and refined by full-matrix least-squares methods (SHELXL).[36] Absorption corrections were conducted by face-indexed or multiscan methods (SADABS).[37] Data collection and final refinement parameters are given in SI Table S2.1. A final analysis of variance between observed and calculated structure factors showed no apparent errors.

**Kinetics of Olefin Face Exchange from Variable-Temperature NMR Simulations.** Simulations of variable temperature $^1$H NMR line shapes (to determine the olefin face exchange rates) were performed with the program WINDNMR.[38] The two methyl proton resonances were chosen for line shape simulations. $^1$H NMR spectra were collected in toluene-$d_8$ at 11 temperatures between 31 and 79 °C.

Before the simulations were performed, the experimental spectra were phased and baseline-corrected using the NUTS software package (Acorn NMR Inc.).[39] The rates of exchange as a function of temperature were determined from visual comparisons of experimental spectra with computed trial line shapes. At each temperature, the exchange rate was the value that gave the best fit of the calculated to observed line shape. For a two-site exchange, the WINDNMR package parametrizes the "rate" of exchange as the sum of the forward and backward rate constants ($k_{ab}$ + $k_{ba}$).[40] For a first-order exchange between two sites of unequal population, the actual rate constants are given by $k_{ab}$ (i.e., leaving the a site) = (mole fraction of the b site)($k_{ab}$ + $k_{ba}$), and similarly for $k_{ba}$. In the olefin decomplexation of **2**, $k_{ab}$ =


https://dx.doi.org/10.1021/acs.organomet.0c00798
Organometallics 2021, 40, 714–724

$k_{ba}$. In addition, the rate of decomplexation is twice the rate of converting one conformer to the other, because the transition state can either generate the original conformer or the new conformer with the same probablility. As a result, the rate of decomplexation $k = 2k_{ab} = k_{ab} + k_{ba}$.

The natural line width (fwhm = 2.2 Hz) was measured from the resonance for the axial methyl group at −13 °C, a temperature at which the exchange is in the slow exchange limit. The natural line width of the equatorial methyl resonance is hard to determine at this temperature due to peak overlapping with small amount of diethyl ether impurity, but subsequent peak fitting at higher temperature suggests that the natural line width of equatorial methyl resonance is smaller than the axial methyl resonance by 0.3 Hz (because the axial methyl peak is broadened due to coupling to the axial $\alpha$- and $\gamma$-$CH_2$ protons, see SI); as a result, the natural line width of equatorial methyl resonance is set to 1.9 Hz. The rate measured from line shape analysis is consistent with the value obtained from spin saturation transfer, which justifies this setting.

The errors in the rate constants of ca. 20% were estimated on the basis of subjective judgments of the sensitivities of the fits to changes in the rate constants. The temperature of the NMR probe was calibrated using a methanol temperature standard,[41] and the estimated error in the temperature measurements was 1 K. Activation parameters were determined by fitting the rates as a function of temperature to the Eyring equation. Uncertainties in the activation parameters were estimated from propagation of error formulas.[42]

**Kinetics of Olefin Face Exchange from Spin Saturation Transfer (SST) Experiments.**[43,44] The rate of olefin face exchange in **2** was measured by monitoring the loss of intensity of the $^1$H NMR resonance of one olefinic resonance of DBCOT of **2** trans to the alkyl group as a function of the presaturation time of irradiation of the other olefinic resonance of DBCOT trans to the alkyl group. The intensity of the former resonance (which we label as site A) is given by the following expression:[43,44]

$$I(t) = \frac{A_4 - A_1}{1 + \frac{A_2}{A_3}} e^{[-t(\frac{1}{A_2} + \frac{1}{A_3})]} + \frac{A_4 - A_1}{1 + \frac{A_3}{A_2}} + A_1$$

where $A_1$ represents the baseline offset, $A_2$ is the lifetime of the hydrogen nuclei in site A, $A_3$ is the spin−lattice relaxation rate of site A, and $A_4$ is the intensity of the site A resonance at $t = 0$. The spin−lattice relaxation rate $A_3$ was measured separately. As discussed above, the measured rate of "alkene flipping"[17] is twice the rate of olefin decomplexation.

**Thermolysis of 2.** A NMR tube containing a solution of $Rh(CH_2CMe_2CH_2CH{=}CH_2)$(DBCOT), **2**, in toluene-$d_8$ was warmed from room temperature to 80 °C over ∼4 h. The solution remains homogeneous: no solid precipitates from solution. The two products of the thermolysis were characterized by their NMR spectra, as follows.

**(Dibenzo[*a*,*e*]cyclooctatetraene)($\eta^3$-*anti*-(1-*tert*-butyl)-propenyl)rhodium(I) (6a).** $^1$H NMR (500 MHz, $C_7D_8$, 20 °C): $\delta$ 5.66 (dd, $^3J_{HH}$ = 8.3 Hz, $J_{RhH}$ = 1.0 Hz, 1 H, =CH— of DBCOT, proximal to *tert*-butyl), 5.62 (dd, $^3J_{HH}$ = 8.3 Hz, $J_{RhH}$ = 3.1 Hz, 1 H, =CH— of DBCOT, distal to *tert*-butyl), 5.61 (dd, $^3J_{HH}$ = 8.3 Hz, $J_{RhH}$ = 3.2 Hz, 1 H, =CH— of DBCOT, proximal to *tert*-butyl), 5.38 (dd, $^3J_{HH}$ = 8.3 Hz, $J_{RhH}$ = 1.0 Hz, 1 H, =CH— of DBCOT, distal to *tert*-butyl), 4.92 (m, 1 H, allyl —CH=), 3.73 (d, 1H, $^3J_{HH}$ = 8.6 Hz, allyl CH−*t*-Bu), 3.40 (ddd, 1 H, $^3J_{HH}$ = 8.4 Hz, $^2J_{HH} \sim J_{RhH} \sim$ 0.9 Hz, =$CH_2$), 2.49 (d, $^3J_{HH}$ = 14.8 Hz, 1 H, =$CH_2$), 0.97 (s, 9 H, *tert*-butyl H). $^{13}$C{$^1$H} NMR (126 MHz, $C_7D_8$, 20 °C): $\delta$ 107.16 (d, $J_{RhC}$ = 5.1 Hz, allyl —CH=), 87.40 (d, $J_{RhC}$ = 8.2 Hz, allyl CH−*t*-Bu), 83.68 (d, $J_{RhC}$ = 13 Hz, distal to *tert*-butyl), 83.5 (overlapped with another peak, = CH— of DBCOT, proximal to *tert*-butyl, identified on HSQC spectrum), 80.72 (d, $J_{RhC}$ = 8.5 Hz, distal to *tert*-butyl), 79.61 (d, $J_{RhC}$ = 9.0 Hz, =CH— of DBCOT, proximal to *tert*-butyl), 62.48 (d, $J_{RhC}$ = 4.0 Hz, =$CH_2$), 33.09 (s, Me). Other resonances, including some quaternary and aromatic resonances, cannot be identified due to peak overlapping or low intensity. The chemical shifts and coupling patterns of the *tert*-butylallyl resonances are similar to those previously reported for a *tert*-butylallyl phosphine complex.[45]

**(Dibenzo[*a*,*e*]cyclooctatetraene)($\eta^3$-*syn*-(1-*tert*-butyl)-propenyl)rhodium(I) (6b).** $^1$H NMR (500 MHz, $C_7D_8$, 20 °C): $\delta$ 5.75 (ABX multiplet, 2H, proximal to *tert*-butyl), 5.40 (dd, $^3J_{HH}$ = 8.3 Hz, $J_{RhH}$ = 2.9 Hz, 1 H, =CH— of DBCOT, distal to *tert*-butyl), 5.36 (dd, $^3J_{HH}$ = 8.3 Hz, $J_{RhH}$ = 1.9 Hz, 1 H, =CH— of DBCOT, distal to *tert*-butyl), 5.30 (m, 1 H, allyl —CH=), 2.95 (d, 1H, $^3J_{HH}$ = 6.9 Hz, =$CH_2$), 2.58 (d, $^3J_{HH}$ = 13.0 Hz, 1 H, allyl CH−*t*-Bu), 1.70 (m, 1 H, =$CH_2$), 1.05 (s, 9 H, *tert*-butyl H). $^{13}$C{$^1$H} NMR (126 MHz, $C_7D_8$, 20 °C): $\delta$ 111.11 (d, $J_{RhC}$ = 5.6 Hz, allyl —CH=), 99.01 (d, $J_{RhC}$ = 6.1 Hz, allyl CH−*t*-Bu), 85.40 (d, $J_{RhC}$ = 12.8 Hz, distal to *tert*-butyl), 82.44 (d, $J_{RhC}$ = 8.7 Hz, distal to *tert*-butyl), 80.32 (d, =CH— of DBCOT, $J_{RhC}$ = 13.6 Hz, proximal to *tert*-butyl), 78.85 (d, $J_{RhC}$ = 9.7 Hz, =CH— of DBCOT, proximal to *tert*-butyl), 56.57 (d, $J_{RhC}$ = 7.9 Hz, =$CH_2$), 31.28 (s, Me). Other resonances, including some quaternary carbon and aromatic resonances, were not identified due to peak overlapping or low intensity.

## ■ ASSOCIATED CONTENT

### Supporting Information

The Supporting Information is available free of charge at https://pubs.acs.org/doi/10.1021/acs.organomet.0c00798.

Crystallographic details with tables of atomic coordinates, displacement parameters, and selected bond distances and angles; $^1$H, $^{13}$C, COSY, HSQC, NMR spectra of M($CH_2CMe_2CH_2CH{=}CH_2$)(diene) complexes **1**−**5**, 1D or 2D NOESY NMR spectra for **1**, **2**, and **4**, and low-resolution mass spectra of **1** and **5**; $^1$H VT-NMR spectra, spectra line shape fitting, SST spectra, intensity change fitting, $T_1$ measurements and Eyring plot for **2**; $^1$H, $^{13}$C, COSY, HSQC, and 1D NOESY NMR spectra of the products formed by thermolysis of **2** (PDF)

### Accession Codes

CCDC 2051827−2051829 contain the supplementary crystallographic data for this paper. These data can be obtained free of charge via www.ccdc.cam.ac.uk/data_request/cif, or by emailing data_request@ccdc.cam.ac.uk, or by contacting The Cambridge Crystallographic Data Centre, 12 Union Road, Cambridge CB2 1EZ, UK; fax: +44 1223 336033.

## ■ AUTHOR INFORMATION


### Corresponding Author

**Gregory S. Girolami** − *School of Chemical Sciences, University of Illinois at Urbana−Champaign, Urbana, Illinois 61801, United States;* orcid.org/0000-0002-7295-1775; Email: girolami@scs.illinois.edu

### Author

**Sumeng Liu** − *School of Chemical Sciences, University of Illinois at Urbana−Champaign, Urbana, Illinois 61801, United States;* orcid.org/0000-0002-2133-2122

Complete contact information is available at: https://pubs.acs.org/10.1021/acs.organomet.0c00798


### Notes

The authors declare the following competing financial interest(s): One patent related to this work has been filed: Metal Complexes for Depositing Films and Method of Making and Using the Same, U.S. Patent 20190077819 (Published Mar. 14th, 2019).

## ■ ACKNOWLEDGMENTS

We thank the National Science Foundation under grants CHE 16-65191 and CHE 19-54745 (to G.S.G.) for support of this research. We thank Dr. Danielle Gray and Dr. Toby Woods of the G. L. Clark X-ray Laboratory at the University of Illinois at Urbana−Champaign for help in collecting the X-ray diffraction data.

## ■ REFERENCES

(1) Vasilyev, V. Y.; Morozova, N. B.; Basova, T. V.; Igumenov, I. K.; Hassan, A. Chemical Vapour Deposition of Ir-Based Coatings: Chemistry, Processes and Applications. *RSC Adv.* **2015**, *5*, 32034−32063.

(2) Garcia, J. R. V.; Goto, T. Chemical Vapor Deposition of Iridium, Platinum, Rhodium and Palladium. *Mater. Trans.* **2003**, *44*, 1717−1728.

(3) Liu, S.; Zhang, Z.; Gray, D.; Zhu, L.; Abelson, J. R.; Girolami, G. S. Platinum ω-Alkenyl Compounds as Chemical Vapor Deposition Precursors. Synthesis and Characterization of $Pt[CH_2CMe_2CH_2CH = CH_2]_2$ and the Impact of Ligand Design on the Deposition Process. *Chem. Mater.* **2020**, *32*, 9316−9334.

(4) Liu, S.; Zhang, Z.; Abelson, J. R.; Girolami, G. S. Platinum ω-Alkenyl Compounds as Chemical Vapor Deposition Precursors. Mechanistic studies of the Thermolysis of $Pt[CH_2CMe_2CH_2CH = CH_2]_2$ in Solution and the Origin of Rapid Nucleation. *Organometallics* **2020**, *39*, 3817−3829.

(5) Bernal Ramos, K.; Saly, M. J.; Chabal, Y. J. Precursor Design and Reaction Mechanisms for the Atomic Layer Deposition of Metal Films. *Coord. Chem. Rev.* **2013**, *257*, 3271−3281.

(6) Shibutami, T.; Kawano, K.; Oshima, N.; Yokoyama, S.; Funakubo, H. Ruthenium Film with High Nuclear Density Deposited by MOCVD Using a Novel Liquid Precursor. *Electrochem. Solid-State Lett.* **2003**, *6*, C117−C119.

(7) Ortuño, M. A.; Conejero, S.; Lledós, A. True and Masked Three-Coordinate T-shaped Platinum(II) Intermediates. *Beilstein J. Org. Chem.* **2013**, *9*, 1352−1382.

(8) DiCosimo, R.; Moore, S. S.; Sowinski, A. F.; Whitesides, G. M. Cyclometalation of Dialkylbis(triethylphosphine)platinum(II) Complexes: Formation of *Pt,Pt*-Bis(triethylphosphine)platinacycloalkanes. *J. Am. Chem. Soc.* **1982**, *104*, 124−133.

(9) Liu, S.; Gray, D.; Zhu, L.; Girolami, G. S. Lithium−Olefin π-Complexes and the Mechanism of Carbolithiation: Synthesis, Solution Behavior, and Crystal Structure of (2,2-Dimethylpent-4-en-1-yl)lithium. *Organometallics* **2019**, *38*, 2199−2210.

(10) Anton, D. R.; Crabtree, R. H. Metalation-Resistant Ligands: Some Properties of Dibenzocyclooctatetraene Complexes of Molybdenum, Rhodium and Iridium. *Organometallics* **1983**, *2*, 621−627.

(11) Appleton, T. G.; Clark, H. C.; Manzer, L. E. The trans-influence: its measurement and significance. *Coord. Chem. Rev.* **1973**, *10*, 335−422.

(12) Ermer, S. P.; Struck, G. E.; Bitler, S. P.; Richards, R.; Bau, R.; Flood, T. C. Kinetics and Conformation in the Reversible Insertion of an Alkene into a Platinum-Carbon Bond in a Chelated (Pentenyl)-platinum Complex. *Organometallics* **1993**, *12*, 2634−2643.

(13) Marcén, S.; Jiménez, M. V.; Dobrinovich, I. T.; Lahoz, F. J.; Oro, L. A.; Ruiz, J.; Astruc, D. Heterodinuclear Iridium Cyclooctadiene Complexes with the $[(\eta^5\text{-}C_5H_5)Fe(\eta^6\text{-}(1,1\text{-di}(2\text{-propenyl})\text{-}3\text{-butenyl})benzene)]^+$ Ligand. *Organometallics* **2002**, *21*, 326−330.

(14) Rahman, A. K. F.; Wilklow-Marnell, M.; Brennessel, W. W.; Jones, W. D. Crystal Structure of Chloridobis[(1,2,5,6-η)-cycloocta-1,5-diene]iridium(I). *Acta. Crystallogr. E* **2017**, *73*, 273−277.

(15) Carpentier, J.-F.; Wu, Z.; Lee, C. W.; Strömberg, S.; Christopher, J. N.; Jordan, R. F. $d^0$ Metal Olefin Complexes. Synthesis, Structures, and Dynamic Properties of $(C_5R_5)_2Zr\text{-}(OCMe_2CH_2CH_2CH = CH_2)^+$ Complexes: Models for the Elusive $(C_5R_5)_2Zr(R)(Olefin)^+$ Intermediates in Metallocene-Based Olefin Polymerization Catalysis. *J. Am. Chem. Soc.* **2000**, *122*, 7750−7767.

(16) Carpentier, J.-F.; Maryin, V. P.; Luci, J.; Jordan, R. F. Solution Structures and Dynamic Properties of Chelated $d^0$ Metal Olefin Complexes $\{\eta^5\text{:}\,\eta^1\text{-}C_5R_4SiMe_2NtBu\}Ti(OCMe_2CH_2CH_2CH = CH_2)^+$ (R = H, Me): Models for the $\{\eta^5\text{:}\,\eta^1\text{-}C_5R_4SiMe_2NtBu\}Ti\text{-}(R')(olefin)^+$ Intermediates in "Constrained Geometry" Catalysts. *J. Am. Chem. Soc.* **2001**, *123*, 898−909.

(17) Stoebenau, E. J.; Jordan, R. F. Nonchelated Alkene and Alkyne Complexes of $d^0$ Zirconocene Pentafluorophenyl Cations. *J. Am. Chem. Soc.* **2006**, *128*, 8638−8650.

(18) Casey, C. P.; Carpenetti, D. W. Measurement of Barriers for Alkene Dissociation and for Inversion at Zirconium in a $d^0$ Zirconium−Alkyl−Alkene Complex. *Organometallics* **2000**, *19*, 3970−3977.

(19) Casey, C. P.; Carpenetti, D. W.; Sakurai, H. Models for Intermediates in Metallocene-Catalyzed Alkene Polymerization: Alkene Dissociation from $Cp_2Zr[\eta^1,\eta^2\text{-}CH_2Si(CH_3)_2CH_2CH = CH_2][B(C_6F_5)_4]$. *Organometallics* **2001**, *20*, 4262−4265.

(20) Wick, D. D.; Goldberg, K. I. C−H Activation at Pt(II) To Form Stable Pt(IV) Alkyl Hydrides. *J. Am. Chem. Soc.* **1997**, *119*, 10235−10236.

(21) Labinger, J. A. Platinum-Catalyzed C−H Functionalization. *Chem. Rev.* **2017**, *117*, 8483−8496.

(22) Yoder, J. C.; Bercaw, J. E. Chain Epimerization during Propylene Polymerization with Metallocene Catalysts: Mechanistic Studies Using a Doubly Labeled Propylene. *J. Am. Chem. Soc.* **2002**, *124*, 2548−2555.

(23) Peng, T. S.; Gladysz, J. A. Mechanism of Equilibration of Diastereomeric Chiral Rhenium Alkene Complexes of the Formula $[(\eta^5\text{-}C_5H_5)Re(NO)(PPh_3)(H_2C = CHR)]^+BF_4^-$. The Metal Traverses Between Alkene Enantiofaces Without Dissociation! *J. Am. Chem. Soc.* **1992**, *114*, 4174−4181.

(24) Budzelaar, P. H. M.; de Gelder, R.; Gal, A. W. A Stable Three-Coordinate Rhodium(I) Olefin Complex. *Organometallics* **1998**, *17*, 4121−4123.

(25) Chaplin, A. B. Rhodium(I) Complexes of the Conformationally Rigid $IBioxMe_4$ Ligand: Isolation of a Stable Low-Coordinate T-Shaped Complex. *Organometallics* **2014**, *33*, 624−626.

(26) Urtel, H.; Meier, C.; Eisenträger, F.; Rominger, F.; Joschek, J. P.; Hofmann, P. A Neutral Three-Coordinate Alkylrhodium(I) Complex: Stabilization of a 14-Electron Species by γ-C−H Agostic Interactions with a Saturated Hydrocarbon Group. *Angew. Chem., Int. Ed.* **2001**, *40*, 781−784.

(27) Corradini, P.; Maglio, G.; Musco, A.; Paiaro, G. Molecular Asymmetry in π-Allylic Complexes of Transition Metals. *Chem. Commun. (London)* **1966**, *0*, 618b−619.

(28) Consiglio, G.; Waymouth, R. M. Enantioselective Homogeneous Catalysis Involving Transition-Metal-Allyl Intermediates. *Chem. Rev.* **1989**, *89*, 257−276.

(29) Solin, N.; Szabó, K. J. Mechanism of the $\eta^3\text{−}\eta^1\text{−}\eta^3$ Isomerization in Allylpalladium Complexes: Solvent Coordination, Ligand, and Substituent Effects. *Organometallics* **2001**, *20*, 5464−5471.

(30) Blanksby, S. J.; Ellison, G. B. Bond Dissociation Energies of Organic Molecules. *Acc. Chem. Res.* **2003**, *36*, 255−263.

(31) Giordano, G.; Crabtree, R. H.; Heintz, R. M.; Forster, D.; Morris, D. E. Di-μ-Chloro-Bis($\eta^4$-1,5-Cyclooctadiene)-Dirhodium(I). *Inorg. Synth.* **1979**, *28*, 88−90.

(32) Abel, E. W.; Bennett, M. A.; Wilkinson, G. Norbornadiene−Metal Complexes and Some Related Compounds. *J. Chem. Soc.* **1959**, *0*, 3178−3182.

(33) Singh, A.; Sharp, P. R. Rh and Ir Dibenzo[a,e]cyclooctatetraene Complexes: Chloro, Hydroxo, and Mixed Au Oxo Complexes. *Inorg. Chim. Acta* **2008**, *361*, 3159−3164.

(34) Crabtree, R. H.; Quirk, J. M.; Felkin, H.; Fillebeen-khan, T. An Efficient Synthesis of $[Ir(cod)Cl]_2$ and Its Reaction with $PMe_2Ph$ to Give *FAC*-$[IrH(PMe_2C_6H_4)(PMe_2Ph)_3]$. *Synth. React. Inorg. Met.-Org. Chem.* **1982**, *12*, 407−413.

(35) APEX3, Bruker AXS, Inc: Madison, Wisconsin, USA., 2018.



https://dx.doi.org/10.1021/acs.organomet.0c00798
*Organometallics* 2021, 40, 714−724

(36) Sheldrick, G. Crystal Structure Refinement with SHELXL. *Acta Crystallogr., Sect. C: Struct. Chem.* **2015**, *71*, 3−8.
(37) Krause, L.; Herbst-Irmer, R.; Sheldrick, G. M.; Stalke, D. Comparison of Silver and Molybdenum Microfocus X-ray Sources for Single-Crystal Structure Determination. *J. Appl. Crystallogr.* **2015**, *48*, 3−10.
(38) Reich, H. J. WinDNMR: Dynamic NMR Spectra for Windows. *J. Chem. Educ.* **1995**, *72*, 1086.
(39) *Nuts*; Acorn NMR Inc., 2012.
(40) Reich, H. J. *WinDNMR help*. https://www.chem.wisc.edu/areas/reich/windnmrhlp/index.htm (accessed 2019/6/10).
(41) Ammann, C.; Meier, P.; Merbach, A. A Simple Multinuclear NMR Thermometer. *J. Magn. Reson.* **1982**, *46*, 319−321.
(42) Morse, P. M.; Spencer, M. D.; Wilson, S. R.; Girolami, G. S. A Static $\alpha$-CH●●●M Interaction Observable by NMR Spectroscopy: Synthesis of the Chromium(II) Alkyl $[Cr_2(CH_2SiMe_3)_6^{2-}]$ and its Conversion to the Unusual 'Windowpane' Bis(metallacycle) Complex $[Cr(\kappa^2CC'\text{-}CH_2SiMe_2CH_2)_2^{2-}]$. *Organometallics* **1994**, *13*, 1646−1655.
(43) Dickinson, P. W. *Trispyrazolylborate and Tetramethylcyclopentadienyl Osmium Chemistry: Toward Methane Coordination Complexes*; University of Illinois at Urbana-Champaign:Urbana, IL, 2005.
(44) Gross, C. L.; Girolami, G. S. Metal−Alkane Complexes. Rapid Exchange of Hydrogen Atoms between Hydride and Methyl Ligands in $[(C_5Me_5)Os(dmpm)(CH_3)H^+]$. *J. Am. Chem. Soc.* **1998**, *120*, 6605−6606.
(45) Werner, H.; Wiedemann, R.; Steinert, P.; Wolf, J. Rhodium(I)-Assisted Stereoselective Coupling of an Alkyl, Aryl or Vinyl Group with a Vinylidene Ligand: A Novel Synthetic Route to $\pi$-Allyl and $\pi$-Butadienyl Rhodium Complexes. *Chem. - Eur. J.* **1997**, *3*, 127−137.

## ■ NOTE ADDED AFTER ASAP PUBLICATION

This paper was published ASAP on March 8, 2021. Additional text and Supporting Information corrections were made and a new version reposted on March 9, 2021.


https://dx.doi.org/10.1021/acs.organomet.0c00798
*Organometallics* 2021, 40, 714−724